Effect of grain size on Hertzian contact damage in 9 mol% Ce-TZP ceramics

Bruno A. Latella[a,*], Tianshun Liu[a], Armand J. Atanacio[b,1]

[a]*Materials Division, Australian Nuclear Science and Technology Organisation, Private Mail Bag 1, Menai, NSW 2234, Australia*
[b]*Department of Chemistry, Materials and Forensic Science, University of Technology, Sydney, PO Box 123, Broadway, NSW 2007, Australia*

Abstract

The Hertzian contact damage in 9 mol% Ce-TZP ceramics with different grain sizes has been investigated. Single-cycle tests were conducted on materials of four grain sizes, 1.1, 1.6, 2.2 and 3 µm. The indentation stress–strain curves for all materials show striking nonlinearity and deviation from the Hertzian elastic response, illustrating a significant quasi-plastic component in the contact damage response. Subsurface damage patterns for these four materials are compared and contrasted using a bonded-interface sectioning technique. The transformation and deformation behaviour, characterised using optical and scanning electron microscopy, of the surface and subsurface regions revealed extensive deformation and compression-driven subsurface damage in the materials. Acoustic emission was used as a complementary technique in order to identify the damage processes during a load–unload cycle. Contact deformation and radial bands extending from the indent impressions due to autocatalytic tetragonal–monoclinic transformation are evident in all except the finest grained (1.1 µm) material. Irrespective of grain size there is no evidence of ring or cone cracking with all material showing hemispherical subsurface damage or yield zones resulting from the stress-induced tetragonal–monoclinic (t–m) transformation with extensive distributed microcracking within these areas for the 1.6, 2.2 and 3 µm grain-size materials. © 2002 Elsevier Science Ltd. All rights reserved.

Keywords: Fracture; Indentation; Mechanical properties; Optical microscopy; Toughness and toughening; ZrO$_2$

1. Introduction

Ceria-stabilised tetragonal zirconia polycrystal (Ce-TZP) ceramics exhibit enhanced fracture toughness and strong crack-resistance (R-curve) behaviour due to the stress-induced tetragonal–monoclinic (t–m) zirconia phase transformation.[1] This same toughening mechanism that imparts strong R-curve behaviour in Ce-TZP ceramics is known to control its damage resistance and fatigue behaviour.[1–5] These toughened Ce-TZP materials have been termed "ductile" because they behave almost like mild-steels. When sufficiently high stresses are applied they develop characteristic bands where tetragonal grains transform to monoclinic zirconia without evidence of cracking. The t–m transformation in Ce-TZPs is unique in that it occurs in bursts and is termed autocatalytic behaviour.[6]

Investigations of Ce-TZP based-ceramics have centred primarily on measuring stress–strain behaviour, strength, transformation zones, fracture toughness and fatigue characteristics using chevron notch, compact tension (CT), double-cantilever beam (DCB), single-edge notch beam (SENB) and bend (three- and four-point) specimens.[2,5,7–9] These techniques are generally deficient in evaluating issues directly pertinent to damage evolution and fracture mechanisms at the grain scale, i.e. short-crack regime, where properties like strength and wear are often determined.

The role of microstructure and the short-crack behaviour of these materials can be examined using Hertzian contact testing (spherical indenters). This technique has been shown to offer useful insights into assessing damage mechanisms and fracture processes on a localised level under concentrated contact loading.[10] Hertzian contact damage studies of zirconia-based ceramics have concentrated primarily on magnesia-partially stabilised zirconia (Mg-PSZ) with controlled microstructures.[11,12] In that work it was shown that the mode of contact damage changes with the heat-treatment from distributed

microcracking in the as-fired (under-aged) to phase transformation in the peak-aged and back to micro-cracking and monoclinic twinning in the over-aged material. Furthermore, the study showed that other damage modes exist along with transformation in Mg-PSZ which has broad implications on fatigue and wear and hence potential applications of these materials. Observations of contact damage in other zirconia materials, namely yttria-stabilised tetragonal zirconia polycrystals (Y-TZP) materials[13] and 12 mol% Ce-TZP ceramics[14] using the Hertzian test have been reported.

In this study the influence of grain size in 9 mol% Ce-TZP ceramics under Hertzian contact damage conditions is investigated in order to identify the micromechanical nature of the damage. The indentation stress–strain responses in all the materials show exaggerated quasi-plasticity irrespective of grain size. Subsurface observations of the contact damage using the bonded-interface technique show a macroscopic damage zone with extensive microcracking.

2. Experimental procedure

The material fabricated was prepared from a CeO_2–ZrO_2 powder containing 9 mol% CeO_2. The powder processing and sintering conditions are described in detail elsewhere.[1] Four Ce-TZP materials with different grain sizes based on the sintering treatments were fabricated, designated Ce-TZP-I, II, III and IV. Grain size measurements by the linear intercept technique gave average values of 1.1, 1.6, 2.2 and 3.0 μm for Ce-TZP-I, II, III and IV, respectively. Essential details of the processing and characterisation of the materials are listed in Table 1. Fig. 1 shows the SEM micrographs of the four Ce-TZP materials as revealed on the fracture surfaces of room temperature strength test samples. The difference in grain size is obvious with a greater degree of inter-granular fracture in the coarser-grained materials.

Surfaces of sintered specimens were prepared for optical and scanning electron microscopy (SEM) by diamond polishing to a 0.25 μm finish. X-ray diffraction (XRD) was used to determine the degree of phase transformation of polished as-fired and annealed specimens. The indentation hardness was evaluated from the impression diagonals of Vickers indentations using a contact load of 100 N. Young's modulus was determined using the impulse excitation technique (Grindo-Sonic MkV, J.W. Lemmens, Belgium).

Indentation stress–strain testing was carried out on polished and gold-coated specimens. Indentations were made using tungsten carbide (WC) spheres of radius $r = 1.2$–12.5 mm, over a load range $P = 200$–3000 N on a universal servo-hydraulic testing machine (Model 8501, Instron, Canton MA) at a fixed crosshead speed of 16.7 μm/s. Residual traces in the gold layer enabled measurement of contact radii (a). Indentation stresses ($p_o = P/\pi a^2$) as a function of indentation strain (a/r) were then determined.

Bonded-interface specimens[15] were used for examining subsurface damage. Indentations were made symmetrically across the traces of the interface at loads from 200–3000 N, with a sphere of radius 3.2 mm. After testing, the bonded specimens were separated and the surfaces and sections cleaned with acetone. The polished sections were subsequently viewed in an optical microscope using Nomarski interference contrast to examine the macroscopic damage patterns. Higher magnification views of the subsurface damage were obtained by scanning electron microscopy (SEM). Raman spectroscopy (Raman II, Bio-Rad) was used as a qualitative check of the t–m transformation from within the subsurface damage regions compared with areas far from it.

Acoustic emission (AE) was used to monitor transformation and damage evolution during indentation loading and unloading. All data were processed by a digital multi-channel system that performs real-time extraction of AE features and acquisition of waveforms (Mistras 2001 AEDSP-32/16, Physical Acoustics, Princeton, NJ). For the AE tests a crosshead speed of 1 μm/s was used with indentation loading to a maximum of 3000 N. A surface profilometer (Alpha-Step 200, Tencor Instruments, Mountain View, CA) was used to estimate the depth and surface feature variations on indents of each material.

3. Results and discussion

Fig. 2 shows the indentation stress–strain curves for single-cycle indentations in the four Ce-TZPs. The data for each material fall on a universal curve, independent of sphere radius, consistent with the principle of geometrical

Table 1
Preparation and properties of 9 mol% Ce-TZP ceramics

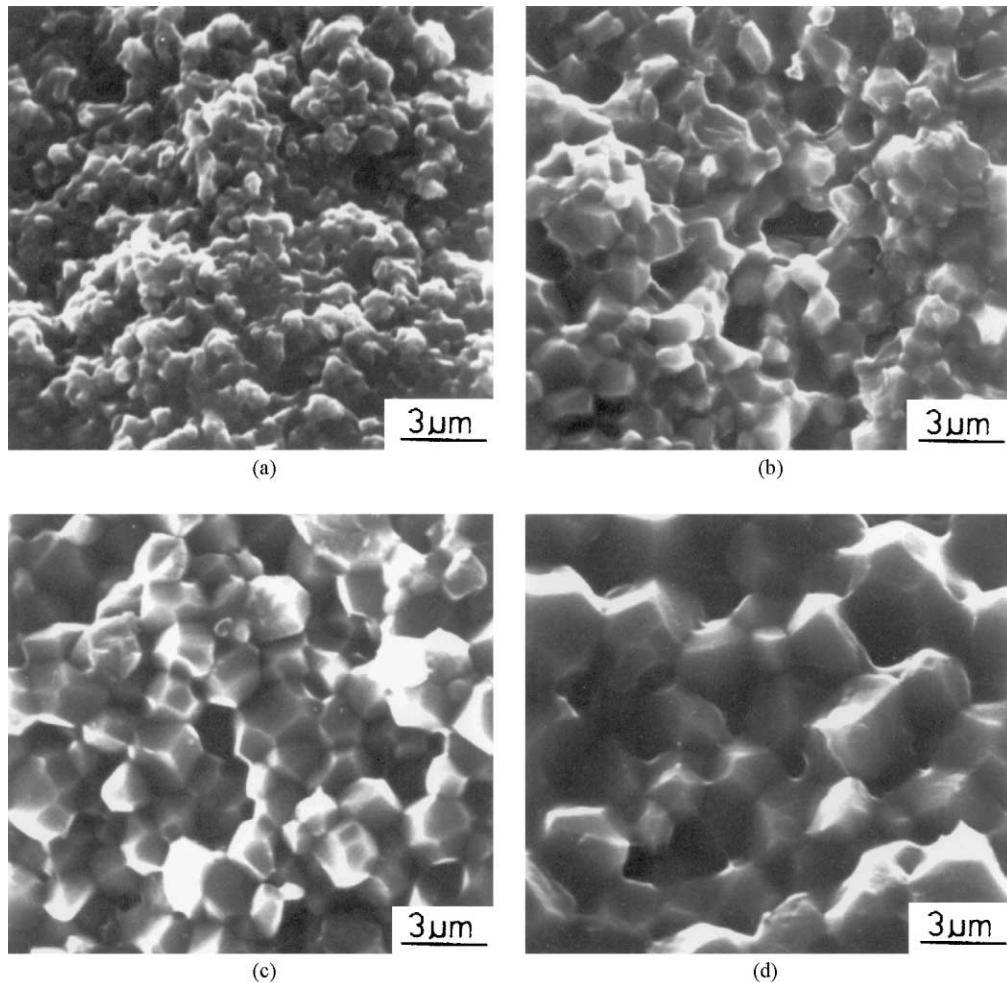| Material	Sintering treatment	Relative density (% TD)	Grain size (μm)	Vickers hardness (GPa)	Young's modulus (GPa)
Ce-TZP-I	1400 °C, 1 h	94	1.1±0.1	6.85±0.33	179±1.85
Ce-TZP-II	1450 °C, 1 h	97	1.6±0.1	7.28±0.19	193±2.75
Ce-TZP-III	1500 °C, 1 h	98	2.2±0.1	7.28±0.08	194±1.76
Ce-TZP-IV	1550 °C, 1 h	97	3.0±0.1	7.11±0.09	197±2.15

Fig. 1. Scanning electron micrographs of the fracture surfaces of (a) Ce-TZP-I (1.1 µm), (b) Ce-TZP-II (1.6 µm), (c) Ce-TZP-III (2.2 µm) and (d) Ce-TZP-IV (3.0 µm). Note the differences in grain size and the extent of intergranular fracture.

similarity.[10] For reference, the inclined solid line represents the Hertzian relation for purely elastic contacts:

$$p_o = (3E/4\pi k)a/r \tag{1}$$

where k is a dimensionless constant:

$$k = (9/16)[(1 - \nu^2) + (1 - \nu_i^2)E/E_i = 0.71 \tag{2}$$

for WC spheres on Ce-TZP-III; where E is Young's modulus, ν is Poisson's ratio and the subscript i denotes the indenter material. The hatched box at the upper right axis represent the Vickers-determined hardness range for the materials (see Table 1 for hardness values of each material). The measured data show a large deviation from the ideal elastic behaviour, indicating significant non-linear deformation (plastic compliance), similar to that observed in other deformable "quasi-plastic" ceramics.[16–18] Irrespective of grain size, the stress-strain response of the materials were quite similar although Ce-TZP-I generally exhibits lower stresses over the strain range that is due to the higher porosity

of this material. It is important to note that even at low indentation stresses and strains all the materials showed visible damage leaving permanent impressions. Hence, the onset of yielding (i.e. plasticity) of the four materials occurs at very low stresses as confirmed by optical microscopy examinations of surface impressions.

Fig. 3 shows surface damage views produced from single-cycle Hertzian indentations in the four materials with a sphere of radius $r = 3.2$ mm and a peak load of 3000 N. For Ce-TZP-I a large residual depression is evident within the contact but there is no sign of ring cracking at the contact periphery. There is minor uplift outside the contact area. For Ce-TZP-II, III and IV the Nomarski contrast micrographs reveal distinct and somewhat striking transformation bands or "star-type" patterns for the most part running radially outwards from the periphery of the surface impression due to the large contact stresses generated from the indentations required to cause t–m transformation. The t–m transformation takes place in a discrete fashion due to the autocatalytic transformation behaviour. These band features occur irregularly with different length scales but
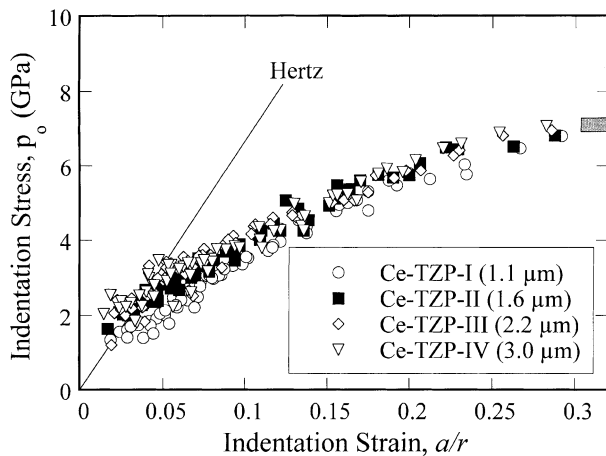
Fig. 2. Indentation stress–strain curve for single cycle contacts for 9 mol% Ce-TZP ceramics of indicated grain size. Solid line is Hertzian elastic response for the 1.6 μm grain size Ce-TZP-II material. Hatched box on right axis is the hardness range of the materials from Vickers indentations.

increase in dimension and intensity with increasing grain size and contact stress. Residual contact depressions are once again evident and there are no ring cracks or any peripheral damage. There is significant surface uplift outside the contact corresponding to a ring of transformed material.

Fig. 4 shows the height variation from several repeat measurements for each material on running a profilometer stylus across the indentations for peak loads of 3000 N ($r = 3.2$ mm). Ce-TZP-I shows a measurable uplift at the periphery of the indent but the width of the impression and the depth are much greater than the other three materials confirming the slightly lower stress-strain response and consistent with the higher porosity of this material compared to the others. For Ce-TZP-II, III and IV the impression widths are equivalent although the depths vary slightly. The uplift outside the impression edges are noticeable and well in excess of that in Ce-TZP-I, and correspond to the t–m transformation rings (see Fig. 3) although the height variation across the bands emanating from these transformation rings are negligible. This was confirmed by running the stylus across individual bands and checking the height variations. It is clear that there is a critical grain size in the 9 mol% Ce-TZPs below which the contact damage mode is somewhat different with the absence of "burst-like" autocatalytic t–m phase transformation in accord with previous work.[4]

Fig. 5 shows plots of cumulative acoustic amplitude versus loading time for one complete loading-unloading cycle on each Ce-TZP ceramic with a peak load of 3000 N. The vertical solid line in the graph delineates between the loading and unloading regions. The acoustic activity increases with increasing grain size, i.e. in the order Ce-TZP-I→Ce-TZP-II→Ce-TZP-III→Ce-TZP-IV, indicating either a greater degree of phase transformation

and/or microcracking. For all materials the acoustic amplitude signals occur predominantly during the loading half-cycle and levels off somewhat on unloading. While Ce-TZP-I with a grain size of 1.1 μm shows overall continuously increasing acoustic activity, the activity occurs more discontinuously in Ce-TZP-II, III and IV with jumps or steps during the loading half-cycle. The "star-like" phase transformations becomes more pronounced with increasing grain size as demonstrated in the surface images shown in Fig. 3 and this correlates well with the highest acoustic activity for Ce-TZP-IV. No "star-like" phase transformations were observed outside the impressions in Ce-TZP-I although transformation does occur in this material.

An important feature of the AE observations is that signals are detected at low indentation loads corresponding to the onset of irreversible deformation and damage. The determination of stress-strain curves, which were based on optical observations of residual impressions provided supporting evidence of the plastic contact and yielding of the materials at low indentation loads. In Ce-TZP-I the acoustic activity occurs solely during the loading half-cycle. By contrast, for Ce-TZP-II, III and IV, there is an appreciable amount of activity observed during the unloading half-cycle, which is ascribed to initiation and/or extension of microcracks (see later). As opposed to the loading half-cycle the continuation of the acoustic amplitude curves for the unloading half-cycle are generally smooth and increase monotonically. Hence, the bulk of the acoustic activity on loading is attributed to t–m transformation with microcrack initiation playing only a minor role based on the difference in the contact damage behaviour and AE results of Ce-TZP-I compared with Ce-TZP-II, III and IV. Optical examinations of the indents used for the AE tests showed that the number of transformation bands decreased slightly in number with increasing grain size although the bands became more prominent (wider and longer): 32 bands for Ce-TZP-II, 30 bands for Ce-TZP-III and 27 bands for Ce-TZP-IV compared with no bands for Ce-TZP-I.

Section views of the subsurface damage patterns in each material obtained from bonded-interface specimens, for $r = 3.2$ mm and $P = 1500$ N, are shown in Fig. 6. In all cases the subsurface damage takes the form of a uplifted distributed hemispherical-shaped yield zone consistent with a quasi-plastic response as indicated by the nonlinear indentation stress-strain curves for each material. Likewise, the damage is concentrated in the region of high compressive stress below the contact. There is no evidence of ring or cone cracks identifiable, not even in the 1.1 μm Ce-TZP-I material, as opposed to other fine-grained non-transformable brittle ceramics.[15,19] The damage zone size is approximately the same for Ce-TZP-II, III and IV and is noticeably smaller in Ce-TZP-I. Overall the subsurface damage
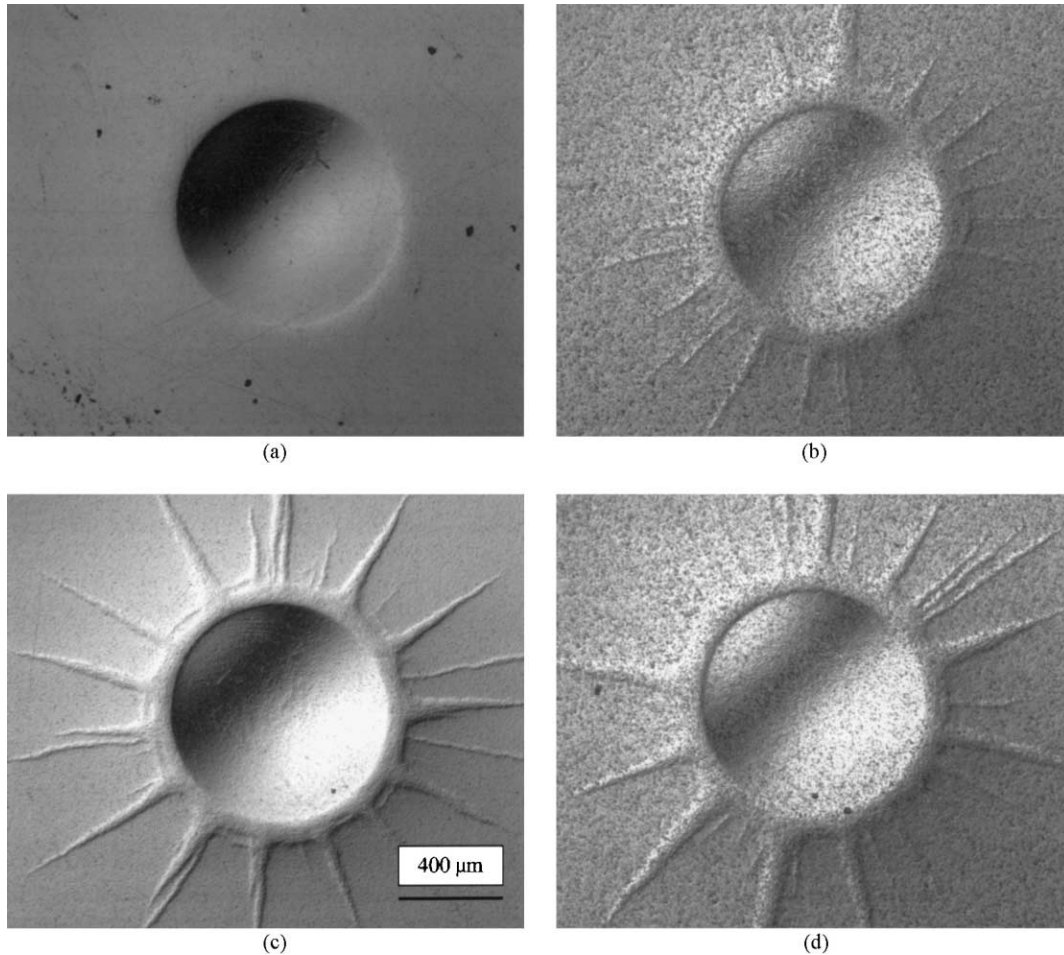
Fig. 3. Surface views (optical micrographs) of Hertzian damage in Ce-TZP, for (a) Ce-TZP-I, (b) Ce-TZP-II, (c) Ce-TZP-III and (d) Ce-TZP-IV viewed in Nomarski illumination. Indentations with WC sphere, radius $r = 3.2$ mm, peak load $P = 3000$ N.

patterns in the four materials are macroscopically similar, indicative of a common compression-shear driving force.[10] It is the shear component that is responsible for initiating the t–m phase transformation.[12]

Fig. 7 shows bonded-interface section views of contact damage in Ce-TZP-II, for loads of 500, 800, 1000 and 2000 N, sphere radius 3.2 mm. The impression diameter and the size of the subsurface damage become more pronounced with increasing indentation load. This trend is typical of all the materials examined. It is worth noting that the damage zone extends from the free contact surface to the highly compressive region below and tends to become more rounded with increasing load.

Fig. 8 shows a typical Raman spectrum for Ce-TZP-III within the subsurface damage zone (for $r = 3.2$ mm, $P = 2500$ N) and an undamaged area. Also included in the plot for identification purposes is the Raman shift spectrum for m-ZrO$_2$. It is clear that there are m-ZrO$_2$ peaks within the damage zone (indicated by m in Fig. 8) signifying t–m phase transformation due to indentation. The m-phase content could not be determined due to the spot size ($\approx$1 mm) of the Raman probe which scans an area that is equivalent to or larger than the size of the

damage area. The spectrum of the undamaged area shows predominantly tetragonal zirconia with indications of some m-ZrO$_2$ peaks. This is expected based on XRD of polished surfaces, which indicated about a 12% m-ZrO$_2$ content. Raman spectroscopy of the subsurface damage zones in all the other materials displayed similar spectra with evidence of monoclinic peaks indicative of indentation induced t–m phase transformation.

High magnification SEM examinations within the subsurface damage zones of the Ce-TZP-II, III and IV materials revealed microcracking, most strongly in Ce-TZP-IV in agreement with the AE data (Fig. 5). No evidence of microcracking was observed in SEM examinations of the damage sites in Ce-TZP-I. For Ce-TZP-II to -IV the extent of microcracking and, therefore, the density of cracks increased with increasing grain size and contact load. Fig. 9 shows SEM micrographs for Ce-TZP-II and Ce-TZP-IV, peak indentation load of 1500 N and sphere radius 3.2 mm. Grain boundary microcracking and an extensive network of intergranular cracks, grain dislodgement and some large cracks at the surrounds of the damage zone were evident but there was no indication of any intragranular shear faults (for
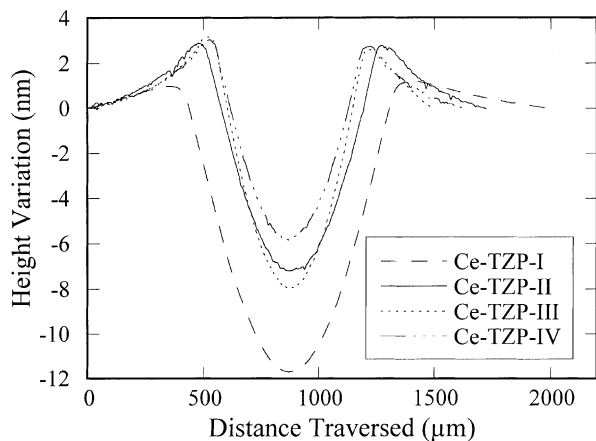
Fig. 4. Surface profilometer traces showing height variations through indentations in Ce-TZP-I, Ce-TZP-II, Ce-TZP-III and Ce-TZP-IV specimens. Indentations with WC sphere, radius $r = 3.2$ mm, peak load $P = 3000$ N.
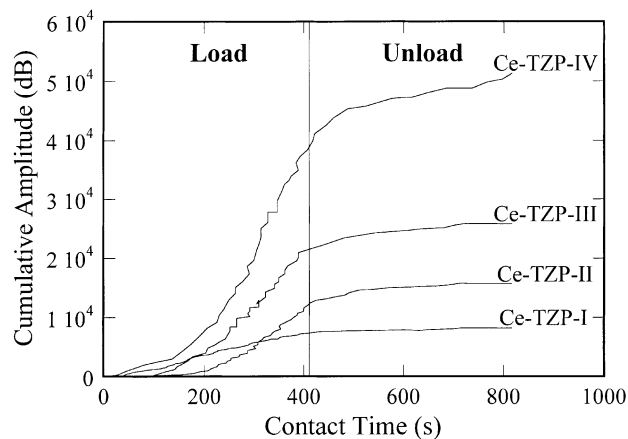

Fig. 5. Cumulative acoustic amplitude versus contact time during indentation load–unload at constant crosshead speed in Ce-TZP-I, Ce-TZP-II, Ce-TZP-III and Ce-TZP-IV specimens, using WC sphere of radius $r = 3.2$ mm at peak load $P = 3000$ N.
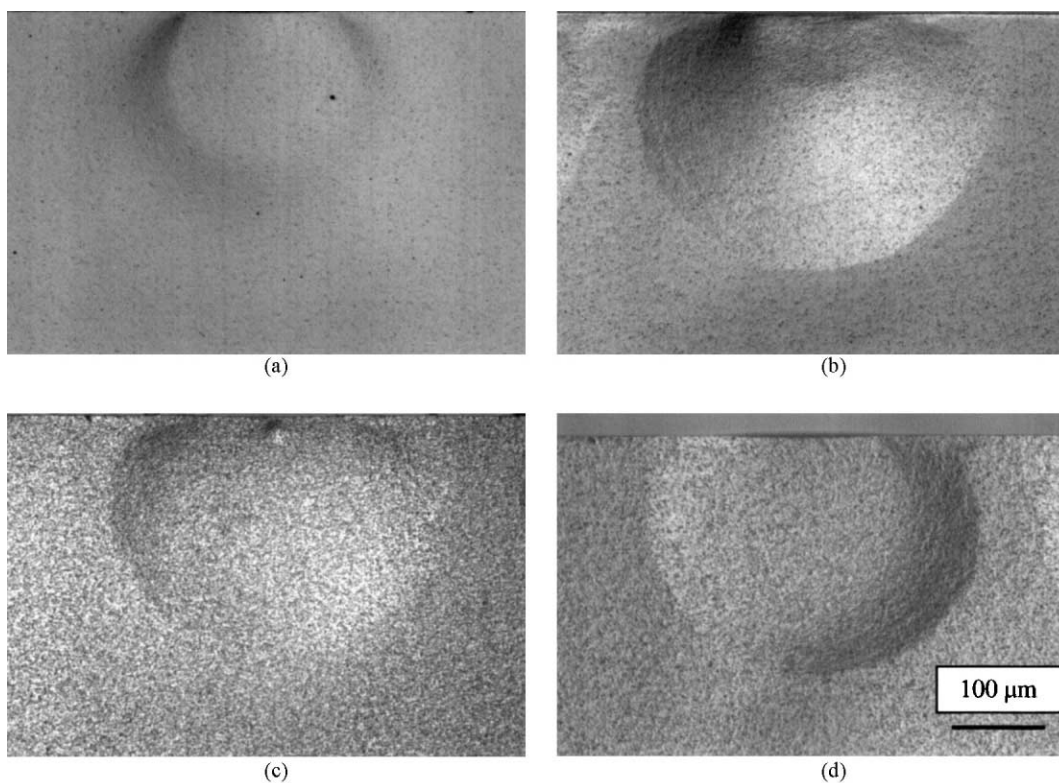

Fig. 6. Subsurface views (optical micrographs) of Hertzian damage in Ce-TZP, for (a) Ce-TZP-I, (b) Ce-TZP-II, (c) Ce-TZP-III and (d) Ce-TZP-IV viewed in Nomarski illumination. Indentations with WC sphere, radius $r = 3.2$ mm, peak load $P = 1500$ N. Sections obtained from the bonded-interface technique.

example, twinning or crystallographic slip planes). From close inspections, the microcracking in the subsurface damage zones tends to be oriented at about 45° to the free surface. At higher indentation loads the microcracks combine to become larger cracks scattered throughout the confined damage region. In some cases large cracks were found at or near the periphery of the damage zones but the majority of microcracking

observed for Ce-TZP-II, III and IV occurred at approximately 100 μm below the surface (for $r = 3.2$ mm and $P = 1500$ N).

The high density of subsurface microcracking observed in Ce-TZP-II to -IV correlates with the high level of acoustic activity that occurs during the unloading half-cycle as indicated in Fig. 5. It is suggested that the compressive contact field and the transformation
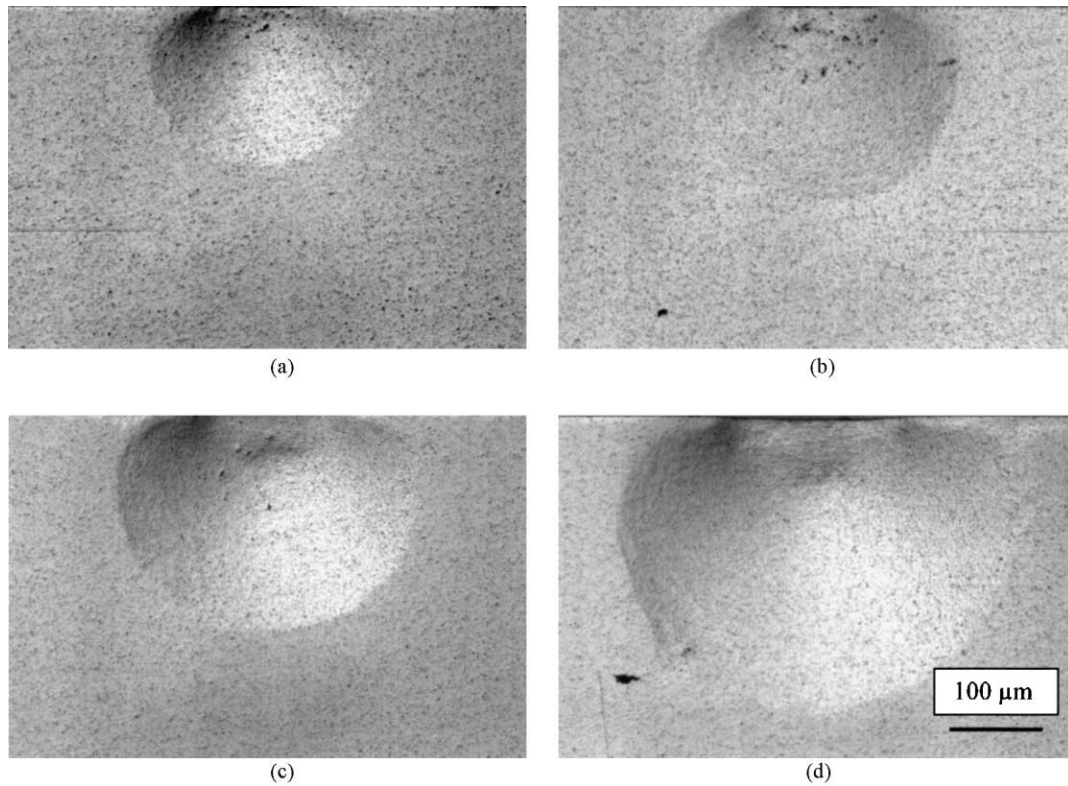
Fig. 7. Subsurface views (optical micrographs) of Hertzian damage in Ce-TZP-II made with WC sphere of radius $r = 3.2$ mm at peak load (a) 500 N, (b) 800 N, (c) 1000 N and (d) 2000 N viewed in Nomarski illumination. Sections obtained from bonded-interface technique.
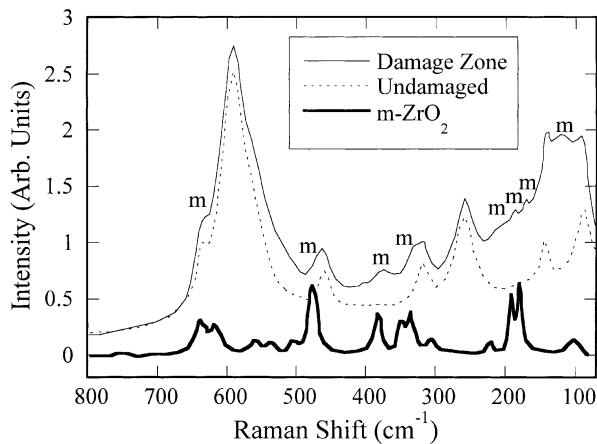

Fig. 8. Raman shift spectra for Hertzian subsurface damage in Ce-TZP-III. Solid curve taken of damage zone site and dashed curve of undamaged area. The monoclinic peaks of the damage zone spectra are marked (m). Included for comparison and identification purposes at the bottom of the graph is the Raman shift spectrum for m-ZrO₂.

process causing expansion of the precipitates which inevitably raises the concentrated compressive stress field further during the loading half-cycle ultimately restricting microcrack initiation and propagation. But on unloading the compressive stress field gradually reduces, so that the majority of microcrack propagation occurs and proceeds much more freely.

The deformation mechanism in the compliant 9 mol% Ce-TZP ceramics involves transformation and then a progressive buildup of microcracking within a distributed damage zone. This involves microscopic brittle processes resulting in a macroscopically "ductile" deformation. The contact damage characteristics of the 1.1 μm Ce-TZP-I material is unlike other homogeneous fine-grained brittle ceramics in that it is susceptible to quasi-plasticity as illustrated by the subsurface damage zone. The burst-like autocatalytic t–m phase transformation is not evident from indentations on Ce-TZP-I as opposed to the 1.6, 2.2 and 3 μm grain-size materials, where these star-shaped bands are quite obvious, even to the naked eye.

The optical and SEM observations in this work have clearly identified the contact damage mechanisms in 9 mol% Ce-TZP ceramics. The t-m transformation is obviously a key element in the damage characteristics of the materials and it is a well-established plasticity mechanism in zirconia-based ceramics.[7] In addition, microcracking is the other damage mode identified in the 1.6, 2.2 and 3 μm grain-size materials, although not in the 1.1 μm material. Thus the Hertzian test has been used as a simple probe for investigating damage and fatigue[20] mechanisms which otherwise may not be amenable using other test methods. A detailed investigation of the cyclic fatigue and strength degradation
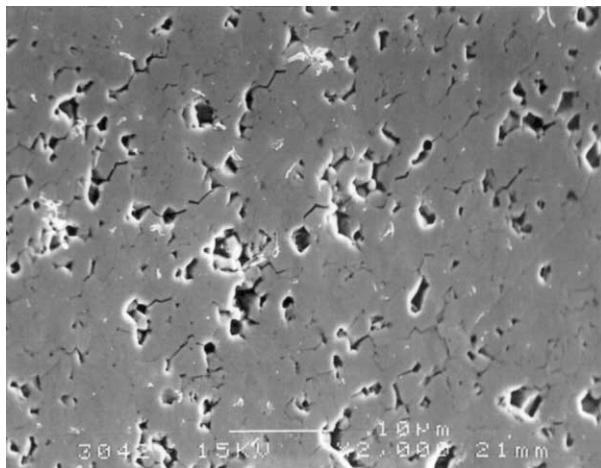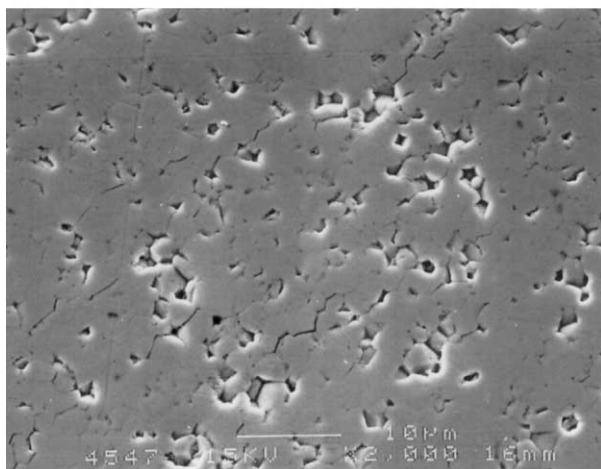
Fig. 9. Scanning electron micrographs of Hertzian damage in (a) Ce-TZP-II and (b) Ce-TZP-IV from Fig. 6.

behaviour of these materials is currently in progress along with a systematic study of the contact damage response of 12 mol% Ce-TZP ceramics[21] that is used widely as grinding media. Likewise, the use of Raman microprobe examination, to obtain quantitative information of the degree of transformation within the subsurface damage zones, is also being investigated further.

4. Conclusion

The present study has examined the influence of grain size on the Hertzian contact damage behaviour of 9 mol% Ce-TZP ceramics. The indentation stress–strain curves indicate a significant non-linear component in the deformation response of the materials irrespective of grain size. This is further exemplified in optical microscopy examinations of the surface contact and subsurface damage regions of each material. The contacts are characterised by discernible surface depression and distributed subsurface damage zones in all materials. Furthermore,

striking surface transformation bands are generated from the indentations in Ce-TZP-II to -IV. Based on AE and Raman spectroscopy measurements the mode of damage is predominantly t–m transformation on loading and microcracking on unloading. The materials all show a discernible damage buildup with increasing load, most prominent in the largest grain-size (3 μm) material. High magnification SEM showed considerable distributed grain boundary microcracking within the subsurface damage zones in Ce-TZP-II to IV. However, no evidence of microcracking was found in the Ce-TZP-I material.

References

1. Grathwohl, G. and Liu, T., Crack resistance and fatigue of transforming ceramics: II, CeO$_2$-stabilised tetragonal ZrO$_2$. *J. Am. Ceram. Soc.*, 1991, **74**, 3028.
2. Liu, T., Mai, Y.-W. and Grathwohl, G., Cyclic fatigue crack propagation behaviour of 9Ce-TZP ceramics with different grain size. *J. Am. Ceram. Soc.*, 1993, **76**, 2601.
3. Liu, S.-Y. and Chen, I.-W., Plasticity-induced fatigue damage in ceria-stabilized tetragonal zirconia polycrystals. *J. Am. Ceram. Soc.*, 1994, **77**, 2025.
4. Liu, T., Mai, Y.-W., Swain, M. V. and Grathwohl, G., Effects of grain size and specimen geometry on the transformation and R-curve behaviour of 9Ce-TZP ceramics. *J. Mater. Sci.*, 1994, **29**, 835.
5. Tsai, J.-F. and Shetty, D. K., Cyclic fatigue of Ce-TZP/Al$_2$O$_3$ composites: role of the degradation of transformation zone shielding. *J. Am. Ceram. Soc.*, 1995, **78**, 599.
6. Reyes-Morel, P. E. and Chen, I.-W., Transformation plasticity of CeO$_2$-stabilised tetragonal zirconia polycrystals: I, stress assistance and autocatalysis. *J. Am. Ceram. Soc.*, 1988, **71**, 343.
7. Green, D. J., Hannink, R. H. J. and Swain, M. V., *Transformation Toughening of Ceramics*. CRC Press, Boca Raton, FL, 1989.
8. Gogotsi, G. A., Zavada, V. P. and Swain, M. V., Mechanical property characterisation of a 9 mol% Ce-TZP ceramic material—I. Flexural response. *J. Eur. Ceram. Soc.*, 1995, **15**, 1185.
9. Gogotsi, G. A., Zavada, V. P. and Swain, M. V., Mechanical property characterisation of a 9 mol% Ce-TZP ceramic material—II. Fracture toughness. *J. Eur. Ceram. Soc.*, 1996, **16**, 545.
10. Lawn, B. R., Indentation of ceramics with spheres: a century after Hertz. *J. Am. Ceram. Soc.*, 1998, **81**, 1977.
11. Pajares, A., Guiberteau, F., Lawn, B. R. and Lathabai, S., Hertzian contact damage in magnesia-partially-stabilized zirconia. *J. Am. Ceram. Soc.*, 1995, **78**, 1083.
12. Pajares, A., Wei, L., Lawn, B. R. and Marshall, D. B., Damage accumulation and cyclic fatigue in Mg-PSZ at Hertzian contacts. *J. Mater. Res.*, 1995, **10**, 2613.
13. Jung, Y.-G., Peterson, I. M., Kim, D. K. and Lawn, B. R., Lifetime-limiting strength degradation from contact fatigue in dental ceramics. *J. Dent. Res.*, 2000, **79**, 722.

14. Lee, S. K., Tandon, R., Readey, M. J. and Lawn, B. R., Scratch damage in zirconia ceramics. *J. Am. Ceram. Soc.*, 2000, **83**, 1428.

15. Guiberteau, F., Padture, N. P. and Lawn, B. R., Effect of grain size on Hertzian contact in alumina. *J. Am. Ceram. Soc.*, 1994, **77**, 1825.

16. Cai, H., Stevens Kalceff, M. A. and Lawn, B. R., Deformation and fracture of mica-containing glass-ceramics in Hertzian contacts. *J. Mater. Res.*, 1994, **9**, 762.

17. Padture, N. P. and Lawn, B. R., Contact fatigue of a silicon carbide with a heterogeneous grain structure. *J. Am. Ceram. Soc.*, 1995, **78**, 1431.

18. Lee, S. K., Wuttiphan, S. and Lawn, B. R., Role of microstructure in Hertzian contact damage in silicon nitride: I. Mechanical characterisation. *J. Am. Ceram. Soc.*, 1997, **80**, 2367.

19. Latella, B. A., O'Connor, B. H., Padture, N. P. and Lawn, B. R., Hertzian contact damage in porous alumina ceramics. *J. Am. Ceram. Soc.*, 1997, **80**, 1027.

20. Latella, B. A. and Liu, T., Transformation and fatigue behaviour of a 9 mol.% Ce-TZP ceramic under Hertzian contact. In *Fatigue 99 International Conference Proceedings*, Vol. 3/4, ed. X. R. Wu and Z. G. Wang, 1999, pp. 1503–1508.

21. Latella, B. A., Hertzian contact damage in 12 mol% Ce-TZP ceramics. Unpublished work, 2001.